nuclear fusion
IAEA

PAPER • OPEN ACCESS

Assessment of the possibility of irradiating tungsten and Cu-alloys in IFMIF-DONES using a realistic specimens configuration

To cite this article: Irene Álvarez *et al* 2025 *Nucl. Fusion* **65** 026058

OPEN ACCESS
IOP Publishing | International Atomic Energy Agency
Nuclear Fusion
Nucl. Fusion **65** (2025) 026058 (10pp)
https://doi.org/10.1088/1741-4326/ada6da

Assessment of the possibility of irradiating tungsten and Cu-alloys in IFMIF-DONES using a realistic specimens configuration

Irene Álvarez[1,*], Marta Anguiano[1], Fernando Mota[2], Rebeca Hernández[3], David Sosa[2], Fabio Moro[4], Simone Noce[4], Yuefeng Qiu[5], Jin Hun Park[5], Frederik Arbeiter[5] and Iole Palermo[2]

[1] Department of Atomic, Molecular and Nuclear Physics, University of Granada, UGR, Granada, Spain
[2] Laboratorio Nacional de Fusión por Confinamiento Magnético, CIEMAT, Madrid, Spain
[3] División de Materiales de Interés energético, CIEMAT, Madrid, Spain
[4] Nuclear Department, ENEA Frascati, Rome, Italy
[5] Karlsruhe Institute of Technology, KIT, Karlsruhe, Germany

E-mail: iac@ugr.es

Received 29 July 2024, revised 21 November 2024
Accepted for publication 7 January 2025
Published 28 January 2025

Abstract
IFMIF-DONES (International Fusion Materials Irradiation Facility-DEMO Oriented NEutron Source) is a facility whose purpose is to obtain data on materials by irradiating them under conditions equivalent to those of the DEMO (DEMOstration) fusion reactor. Tungsten and CuCrZr alloy are two candidate materials to be used in DEMO, tungsten for the first wall and divertor (DIV) and CuCrZr alloy for the DIV. So, studying the behavior of these materials in IFMIF-DONES facility and comparing the results with the DEMO environment is crucial. In the high flux test module in IFMIF-DONES has been considered a realistic distribution of specimens. The IFMIF-EVEDA beam have been used with a footprint size of 20×5 cm^2, the nominal energy is 40 MeV with a current of 125 mA, for the calculation other energies have been considered 25, 30 and 35 MeV. The results of IFMIF-DONES have been compared with different DEMO concepts, Dual Coolant Lithium Lead, Water Cooled Lithium Lead and Helium Cooled Pebble Bed. In general, the primary displacement damage rate meets between IFMIF-DONES and DEMO, while the gas production is at the limit for W and fulfilled for the CuCrZr alloy.

Keywords: IFMIF-DONES, neutronics, comparative, DEMO, DPA, gas-production

(Some figures may appear in colour only in the online journal)

* Author to whom any correspondence should be addressed.

1. Introduction

The first wall (FW) and the divertor (DIV) of the future DEMOnstration power plant (DEMO) will receive high heat and particle fluxes from the plasma. So, the materials chosen for these areas must be sufficiently resistant to these outstanding conditions. Tungsten (W) and CuCrZr alloy (Cu–1.1Cr–0.1Zr) are two of the materials considered for nuclear fusion reactors due to their physical properties that make them suitable for withstanding the extreme conditions present in a fusion environment.

Tungsten has a high melting point, allowing it to withstand high temperatures. Moreover, exhibits good resistance to radiation, making it suitable for use in nuclear fusion environments where radiation is a significant concern. It has a low neutron absorption cross-section, meaning it does not absorb a significant amount of neutrons, helping to prevent radioactive activation issues. And in addition to having good thermal conductivity, it has an excellent anti-plasma sputtering and low tritium retention [1, 2].

In the CuCrZr alloy, copper is known for its excellent thermal and electrical conductivity, aiding in dissipating heat generated in the reactor. The addition of chromium and zirconium enhances the mechanical strength of copper, making it suitable for resisting mechanical stresses and thermal cycles. The CuCrZr alloy has good ductility, and is corrosion-resistant, crucial for ensuring a long lifespan of the material in a nuclear fusion environment [3–6].

Both tungsten and CuCrZr alloy present high resistance to radiation damage and fracture toughness, so they are among the leading candidate materials for DEMO [7, 8]. Moreover, the CuCrZr alloy is essential to facilitate the extraction of all the power received and transmit it to cooling He channel.

These two interesting materials have been analysed in this paper to compare different material irradiation effects parameters in the extreme irradiation environments of the fusion reactor DEMO and IFMIF-DONES (International Fusion Materials Irradiation Facility-DEMO Oriented NEutron Source) [9–11]. IFMIF-DONES is a deuteron source with 40 MeV and 125 mA (7.8×10^{17} s^{-1}). A flux of 6.8×10^{16} neutrons s^{-1} [12] with an energy up to 14 MeV are generated through the reaction of deuterons with lithium, $D^{+}+^{6,7}Li$. The footprint of this neutron source is 20×5 cm^2.

Depending on the design of the breeding blanket, there are different DEMO concepts. Three different DEMO concepts have been selected for this assessment, the Dual Coolant Lithium Lead (DCLL) developed by CIEMAT [13, 14], the Water Cooled Lithium Lead (WCLL) by ENEA [15, 16] and Helium Cooled Pebble Bed (HCPB) by KIT [17–19]. The power of all the DEMO concepts is 1998 MW. The DCLL and WCLL have a liquid breeding blanket and the HCPB has a solid one.

The neutron spectrum and the material under irradiation are fundamental parameters for determining the rate of primary displacement damage. Thus, the primary displacement damage rate varies depending on the specific material irradiated and the irradiation conditions. This rate is measured in displacements per atom (dpa), excluding other bulk material processes such as recombination, migration, or clustering effects. In addition, the transmutation-driven production of helium and hydrogen, relative to the number of point defects, is also crucial for understanding radiation effects in materials [20]. The damage dose rate directly influences the extent of primary displacement damage caused by neutron interactions. The ratios of helium and hydrogen production to damage dose also significantly affect defect diffusion and damage evolution pathways [20]. For simplicity, these ratios will be referred to as the He and H ratios, respectively, throughout this paper.

Furthermore primary displacement damage ratio, He and H gas production have been obtained for each material in IFMIF-DONES and DEMO to compare both environments. It should be noted that in order to design an irradiation experiment in IFMIF-DONES equivalent to the irradiation conditions expected in DEMO, the gas production to damage dose rate would be on the same line.

2. Methodology

2.1. Materials and geometry models

Neutron spectrum for DCLL, WCLL and HCPB has been calculated in the FW and DIV. EUROFER97 is considered to be in the FW and CuCrZr alloy for the DIV. W is considered in both parts. Neutron fluence rate, primary displacement damage rate (arc_dpa, NRT_dpa) and gas production have been calculated for each case so it can be compared with the data obtained in IFMIF-DONES. The results for EUROFER97 have been published in previous works [21–23].

All these parameters have been calculated from the neutron spectrum, to do that, this neutron spectrum is considered as the neutron source in a simplified MCNP geometry with two concentric spheres. The key assumptions for conducting these calculations are as follows: firstly, the neutron source emanates from a spherical surface with an area of 1 cm^2, as the neutron spectrum is provided in $ncm^{-2}\,s^{-1}$. Secondly, the response functions are tallied within a thin spherical shell to minimize neutron spectrum attenuation. The radius of the inner sphere is 0.289 02 cm, while that of the concentric sphere is 0.4 cm. Despite efforts to minimize attenuation, some loss is inevitable; thus, the response functions are normalized to account for these losses. The neutron spectrum for each case is shown in figure 1. To compare the neutron spectra of DEMO with DONES, two positions inside the high flux test module (HFTM) [21, 24] have been selected. The rig 45 and 13 are in central part, the first one in the first line of the beam, while the second one is in the last line (figure 2). These two positions give us the range of spectra in the IFMIF-DONES.

The specimens model considered within the HFTM in IFMIF-DONES is the CLC.v2.0 presented in figure 3, and previously analysed in [23]. This model can be divided into three essential parts, the container box, the specimens and the customed filler blocks. The container box cannot be made of either CuCrZr alloy or tungsten, so it is best to make it out

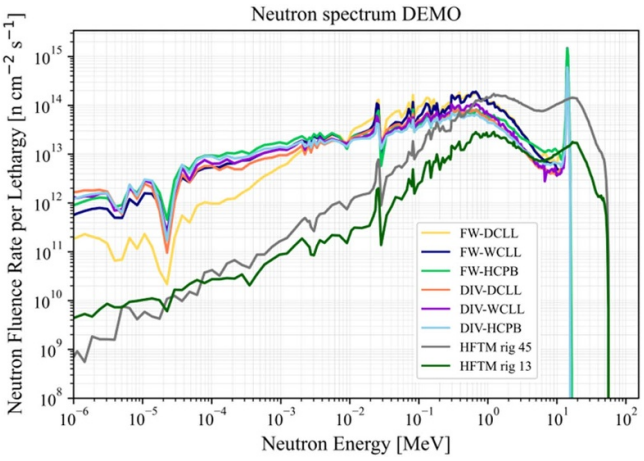

Figure 1. Neutron spectra of the different DEMO concepts considered, DCLL, WCLL, and HCPB and compared to the neutron spectra obtained in the rigs 13 and 45 inside the HFTM.

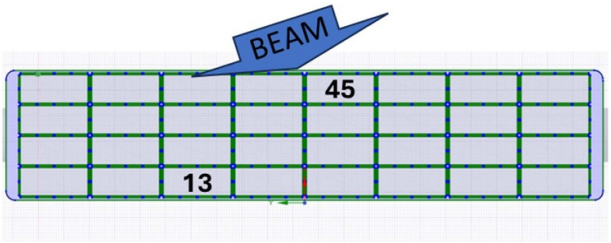

Figure 2. Distribution of the numeration for the rigs inside the HFTM.

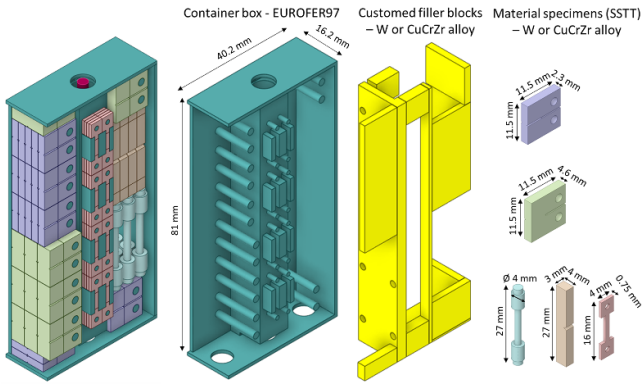

Figure 3. CLC.v2.0 model packaging proposal of SSTT in the HFTM specimen stack.

of EUROFER97, which is an already designed case model and is another of the main materials to be tested in IFMIF-DONES. The container box takes a 29.33% of volume of the specimen stack. The specimens and the customed filler blocks are the parts to be changed to tungsten and CuCrZr alloy. CLC.v2.0 is the referenced model because it has a good proportion of material to be tested (56.5%) and sodium (12.92%). The specimens inside this model have been designed with Small Specimen Test Techniques (SSTTs) [25]. The test cell model of IFMIF-DONES used is 'mdl9.2.8'.

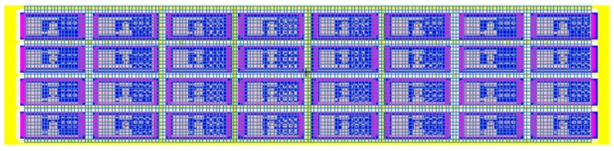

Figure 4. Horizontal cross section of the HFTM in the specimens region mesh for the CLC.v2.0 model.

2.2. Neutron transport calculation methodology

For the neutron transport calculations, the McDelicious code based on MCNP6.2 [26] has been used to reproduce the IFMIF deuteron–lithium neutron source [27]. The results shown in this paper take into account the 20 × 5 cm^2 IFMIF-EVEDA beam footprint. Various deuteron energies have been considered to compare different scenarios. The nominal energy is 40 MeV, but also 25, 30, 35 MeV are presented, to cover the full range of operation energies. The nuclear data library used for neutron transport calculations is FENDL.3.1d [28].

The irradiation parameters presented are primary displacement damage rate and He and H production to displacement damage dose ratios. Gas production to damage dose ratio is essential to understand the effects of radiations in the materials [20] as commented in introduction section. The response functions have been integrated for full power year [fpy] of 365.25 d per year.

Two methodologies have been considered to obtain the primary displacement damage rate, the Norgett Robinson Torrens (NRT) [29] and arc_DPA methods [30]. The design of neutron irradiation experiments has traditionally relied on the NRT model to estimate radiation levels. This model adjusts only four elements—Cu, Fe, Au, and W—and does not account for defect recombination or cluster formation. Recently, however, a new concept, known as the arc-dpa method, was introduced within the IAE CRP project 'Primary Radiation Damage Cross Sections'. This approach incorporates defect recombination during the thermal spike phase, utilizing molecular dynamics simulations across a broad range of elements relevant to nuclear fusion research. Despite this advancement, the NRT model remains crucial for consistency with past calculations, while the arc-dpa concept serves to build an updated database on primary displacement damage. The JEFF3.3DPAarc nuclear data library [31] supports both NRT and arc-dpa calculations for primary displacement damage. The calculation of H and He production have been done integrating the neutron spectrum with gas production cross section MT203 for H and MT207 for He from the nuclear data library FENDL.3.1d. For simplicity, we refer to He and H ratios instead of He and H production to damage dose ratios.

A mesh that covers all the HFTM capsules area has been used for the presentation of the different response function. The resolution of this mesh is 2.5 × 2.5 × 2.5 mm^3. In figure 4 can be seen this mesh for the detailed model CLC.v2.0.

The elements composition considered for this study are in tables 1 and 2. The first one corresponds to W. The principal element is the W with a 99.96% and Mo with 0.01%, the rest of the elements do not reach the 0.005%.

Table 1. W isotopic composition [32].

Element	Weight %	Density (atoms cm^{-3})	Density (g cm^{-3})
W	99.95	$6.237 \cdot 10^{22}$	1.8992
Mo	0.01	$6.24 \cdot 10^{18}$	0.0019
C	0.003	$1.87 \cdot 10^{18}$	0.000 57
Fe	0.003	$1.87 \cdot 10^{18}$	0.000 57
O	0.002	$1.25 \cdot 10^{18}$	0.000 38
Si	0.002	$1.25 \cdot 10^{18}$	0.000 38
P	0.002	$1.25 \cdot 10^{18}$	0.000 38
Cr	0.002	$1.25 \cdot 10^{18}$	0.000 38
Ta	0.002	$1.25 \cdot 10^{18}$	0.000 38
Al	0.0015	$9.36 \cdot 10^{17}$	0.000 285
Na	0.001	$6.24 \cdot 10^{17}$	0.000 19
K	0.001	$6.24 \cdot 10^{17}$	0.000 19
Co	0.001	$6.24 \cdot 10^{17}$	0.000 19
Cu	0.001	$6.24 \cdot 10^{17}$	0.000 19
Nb	0.001	$6.24 \cdot 10^{17}$	0.000 19
Ag	0.001	$6.24 \cdot 10^{17}$	0.000 19
H	0.0005	$3.12 \cdot 10^{17}$	$9.5 \cdot 10^{-5}$
N	0.0005	$3.12 \cdot 10^{17}$	$9.5 \cdot 10^{-5}$
Mg	0.0005	$3.12 \cdot 10^{17}$	$9.5 \cdot 10^{-5}$
S	0.0005	$3.12 \cdot 10^{17}$	$9.5 \cdot 10^{-5}$
Ca	0.0005	$3.12 \cdot 10^{17}$	$9.5 \cdot 10^{-5}$
Ti	0.0005	$3.12 \cdot 10^{17}$	$9.5 \cdot 10^{-5}$
As	0.0005	$3.12 \cdot 10^{17}$	$9.5 \cdot 10^{-5}$
Mn	0.0005	$3.12 \cdot 10^{17}$	$9.5 \cdot 10^{-5}$
Ni	0.0005	$3.12 \cdot 10^{17}$	$9.5 \cdot 10^{-5}$
Zn	0.0005	$3.12 \cdot 10^{17}$	$9.5 \cdot 10^{-5}$
Zr	0.0005	$3.12 \cdot 10^{17}$	$9.5 \cdot 10^{-5}$
Cd	0.0005	$3.12 \cdot 10^{17}$	$9.5 \cdot 10^{-5}$
Ba	0.0005	$3.12 \cdot 10^{17}$	$9.5 \cdot 10^{-5}$
Pb	0.0005	$3.12 \cdot 10^{17}$	$9.5 \cdot 10^{-5}$
Total	100	$6.24 \cdot 10^{22}$	19

In the case of the CuCrZr alloy, the 98.52% is Cu, 0.9% is Cr and 0.15% is Zr. The rest of the elements have 0.1% or lower. The element composition used for this alloy is presented in table 2.

Table 2. CuCrZr alloy isotopic composition [31].

Element	Weight %	Density (atoms cm^{-3})	Density (g cm^{-3})
Cu	98.19	$8.31 \cdot 10^{22}$	8.74
Cr	1.10	$9.28 \cdot 10^{20}$	0.098
Zr	0.10	$8.81 \cdot 10^{19}$	0.009
O	0.13	$1.07 \cdot 10^{20}$	0.011
Nb	0.07	$5.77 \cdot 10^{19}$	0.006
Ni	0.06	$5.48 \cdot 10^{19}$	0.006
Co	0.05	$4.55 \cdot 10^{19}$	0.005
Mg	0.10	$8.82 \cdot 10^{19}$	0.009
Si	0.09	$7.63 \cdot 10^{19}$	0.008
Fe	0.02	$1.92 \cdot 10^{19}$	0.002
P	0.03	$2.42 \cdot 10^{19}$	0.003
As	$8.45 \cdot 10^{-3}$	$7.15 \cdot 10^{18}$	$7.52 \cdot 10^{-4}$
S	$7.90 \cdot 10^{-3}$	$6.69 \cdot 10^{18}$	$7.03 \cdot 10^{-4}$
Al	$7.04 \cdot 10^{-3}$	$5.96 \cdot 10^{18}$	$6.27 \cdot 10^{-4}$
B	$5.86 \cdot 10^{-3}$	$4.96 \cdot 10^{18}$	$5.21 \cdot 10^{-4}$
Sb	$5.72 \cdot 10^{-3}$	$4.84 \cdot 10^{18}$	$5.09 \cdot 10^{-4}$
Sn	$5.34 \cdot 10^{-3}$	$4.52 \cdot 10^{18}$	$4.75 \cdot 10^{-4}$
Zn	$4.92 \cdot 10^{-3}$	$4.17 \cdot 10^{18}$	$4.38 \cdot 10^{-4}$
Ta	$3.50 \cdot 10^{-3}$	$2.96 \cdot 10^{18}$	$3.12 \cdot 10^{-4}$
Pb	$3.06 \cdot 10^{-3}$	$2.59 \cdot 10^{18}$	$2.72 \cdot 10^{-4}$
Mn	$2.31 \cdot 10^{-3}$	$1.95 \cdot 10^{18}$	$2.05 \cdot 10^{-4}$
Bi	$9.09 \cdot 10^{-4}$	$7.69 \cdot 10^{17}$	$8.09 \cdot 10^{-5}$
Total	100	$8.46 \cdot 10^{22}$	8.9

Table 3. Calculated parameters for tungsten in the first wall of the different DEMO concepts.

	Tungsten-first wall		
	DCLL	WCLL	HCPB
Neutron fluence rate [$ncm^{-2}\ s^{-1}$]	$6.75 \cdot 10^{14}$	$6.22 \cdot 10^{14}$	$4.20 \cdot 10^{14}$
H production [H appm/fpy]	8.59	8.64	8.48
He production [He appm/fpy]	3.65	3.67	3.62
Primary displacement damage rate [arc_dpa/fpy]	1.05	0.98	0.78
Primary displacement damage rate [NRT_dpa/fpy]	5.12	4.96	4.21
H ratio [H appm/NRT_dpa]	1.68	1.74	2.01
He ratio [He appm/NRT_dpa]	0.71	0.74	0.86
H ratio [H appm/arc_dpa]	8.21	8.76	10.6
He ratio [He appm/arc_dpa]	3.49	3.72	4.55

3. Results

In the first part of this section, we show the data obtained for DEMO and in the second part they are compared with the corresponding ones obtained for IFMIF-DONES.

3.1. DEMO

In this section, the data obtained for different DEMO configurations (DCLL, WCLL, HCPB) are shown in tables 3–5.

In table 3 results obtained using tungsten in the FW are shown, while the equivalent ones in the DIV are shown in table 4. The data for primary displacement damage ratio is in general a bit lower in the case of the DIV, around 2 [NRT_dpa/fpy], than in the FW, around 4 [NRT_dpa/fpy], probably because the neutron fluence rate is lower too. The data for the He ratio is very low, in fact less than 1 [He appm/NRT_dpa] in any of the cases. In the case of H ratio, the values are between 1–2 [H appm/NRT_dpa]. The arc_dpa/fpy is also a little bit lower in the DIV, around 0.5 [arc_dpa/fpy] than in the FW, around 1 [arc_dpa/fpy]. So, the gas ratios calculated using arc_dpa, are higher than the NRT_dpa data, but always follow the same trend. The H ratio is around 6.6–10 [H appm/arc_dpa] and 2.8–4.5 [He appm/arc_dpa] for the case of He.

In case of the CuCrZr alloy, the data in the DIV are in table 5. Primary displacement damage is very similar in all cases, around 7 [NRT_dpa/fpy]. The H rate gas production is around 3.4 [H appm/NRT_dpa] and He rate is 6.6 [He appm/NRT_dpa]. Taking into account the arc_dpa calculation, the data of primary displacement rate is around 1.2

Table 4. Calculated parameters for tungsten in the divertor of the different DEMO concepts.

	Tungsten-divertor		
	DCLL	WCLL	HCPB
Neutron fluence rate [ncm^{-2} s^{-1}]	$3.75 \cdot 10^{14}$	$4.08 \cdot 10^{14}$	$3.43 \cdot 10^{14}$
H production [H appm/fpy]	3.38	3.33	3.54
He production [He appm/fpy]	1.45	1.43	1.53
Primary displacement damage rate [arc_dpa/fpy]	0.47	0.50	0.45
Primary displacement damage rate [NRT_dpa/fpy]	2.19	2.35	2.19
H ratio [H appm/NRT_dpa]	1.54	1.42	1.62
He ratio [He appm/NRT_dpa]	0.66	0.61	0.70
H ratio [H appm/arc_dpa]	7.22	6.61	7.98
He ratio [He appm/arc_dpa]	3.11	2.84	3.44

Table 5. Calculated parameters for CuCrZr alloy in the first wall of the different DEMO concepts.

	CuCrZr alloy-divertor		
	DCLL	WCLL	HCPB
Neutron fluence rate [ncm^{-2} s^{-1}]	$3.75 \cdot 10^{14}$	$4.08 \cdot 10^{14}$	$3.43 \cdot 10^{14}$
H production [H appm/fpy]	261.50	260.52	277.89
He production [He appm/fpy]	48.55	47.65	5.06
Primary displacement damage rate [arc_dpa/fpy]	1.19	1.30	1.12
Primary displacement damage rate [NRT_dpa/fpy]	7.30	7.55	7.01
H ratio [H appm/NRT_dpa]	35.85	34.49	39.62
He ratio [He appm/NRT_dpa]	6.65	6.31	7.07
H ratio [H appm/arc_dpa]	219.15	200.22	246.22
He ratio [He appm/arc_dpa]	40.68	36.62	44.49

[arc_dpa/fpy], the H ratio 2.0–2.5 [H appm/arc_dpa] and the He ratio 3.6–4.4 [He appm/arc_dpa].

All results presented in tables 3–5 have an uncertainty lower than 2%, so based on [25], is considered a quality result.

3.2. Comparation with IFMIF-DONES

In this section we show the comparison between the results obtained for DEMO in the previous section and the equivalent ones in IFMIF-DONES. For this comparation, primary displacement damage and gas production (He and H) to displacement damage dose ratios for the CLC.v2.0 have been obtained for each material under study.

3.2.1. Tungsten. The neutron fluence rate at the midpoint of the beam footprint has been calculated and it is shown in figure 5. The neutron fluence rate in the first four central rigs reach a value around $5 \cdot 10^{14}$ ncm^{-2} s^{-1}, decreasing to $2 \cdot 10^{13}$ ncm^{-2} s^{-1} in the furthest rigs. The neutron fluence rate does not change a lot with respect of using EUROFER97 specimens [22, 23] because the volume considered for the

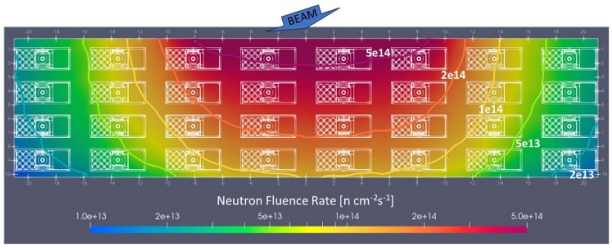

Figure 5. Horizontal cross section of the neutron fluence rate maps [ncm^{-2} s^{-1}] of CLC.v2.0 at the middle of the deuteron beam with tungsten as specimen material.

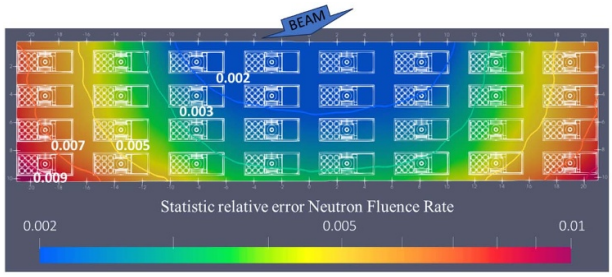

Figure 6. Horizontal cross section of the statistic relative error of the neutron fluence rate maps of the CLC.v2.0 model at the middle of the 20 × 5 cm^2 deuteron beam footprint size using W as specimens material.

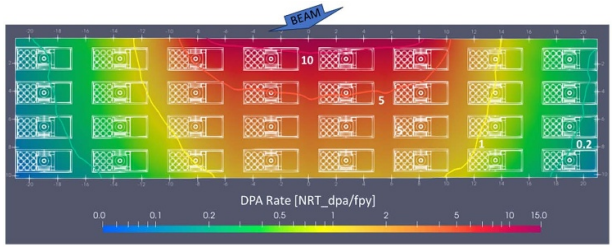

Figure 7. Horizontal cross section of the primary displacement damage rate [NRT_dpa/fpy] of the CLC.v2.0 specimen stacks at the middle of the deuteron beam with tungsten as specimen material.

study is small, although the absorption of the neutron is different depending on the material.

The statistic relative error for the 20 × 5 cm^2 beam footprint using tungsten as material for the specimens in the CLC.v2.0 model is shown in figure 6. Therefore, based on [23], it is considered a quality, as it is less than 1%.

In figure 7 the results for the displacement damage rate are shown. The NRT_dpa values are in the range from 0.2 to 11 NRT_dpa/fpy. Previous calculation [33] for tungsten in the HFTM of IFMIF-DONES provided a maximum value of NRT_dpa/fpy of 5. The discrepancy between the ranges is due to the effective threshold displacement energies used. The minimum kinetic energy required for an atom in a solid to be permanently displaced from its lattice site to a defect position is known as the threshold displacement energy. To eliminate discrepancies in the calculation of NRT_dpa that arose among different authors, due to the arbitrariness in selecting the minimum displacement energy, currently is used

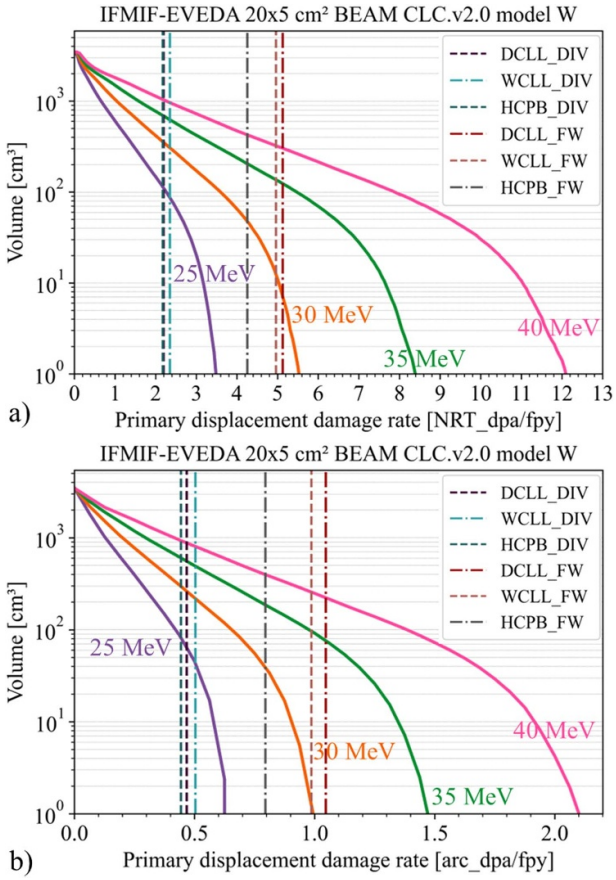

Figure 8. Available integrated irradiation volume (32 rigs) versus primary damage dose rate [dpa/fpy] for the CLC.v2.0 model for 20, 30, 35, 45 MeV energy beam and the values expected for each DEMO concept. (*a*) [NRT_dpa/fpy]; (*b*) [arc_dpa/fpy].

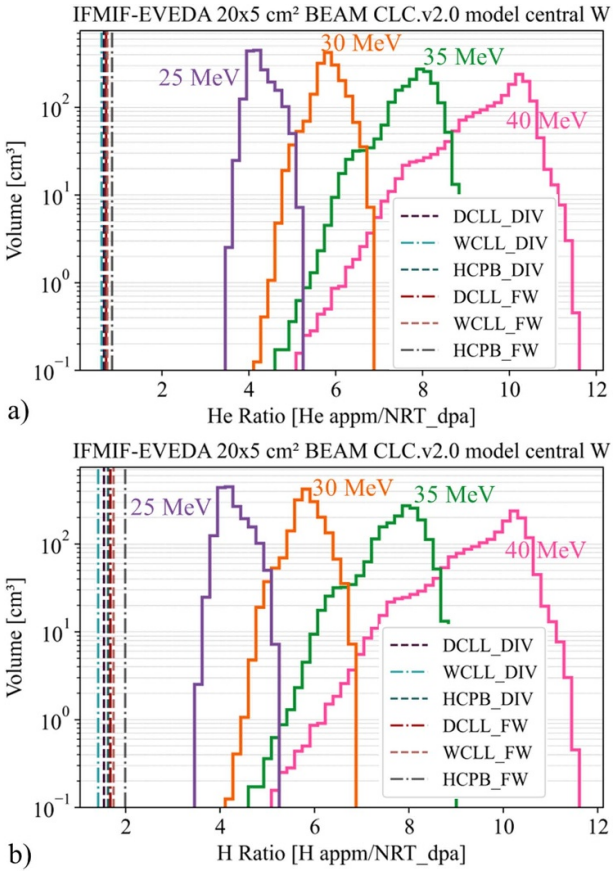

Figure 9. Central irradiation volumes as function of He-DPA (panel (*a*)) and H-DPA (panel (*b*)) ratio for the CLC.v2.0 model for 20, 30, 35, 45 MeV energy beam and the values expected for each DEMO concept considering the four central rigs.

the library JEFF3.3DPAarc to determine both the arc_DPA and NRT_dpa, as commented above. In this nuclear data library, for the NRT_dpa model, a specific threshold displacement energy was selected for each element based on molecular dynamic calculations found in the bibliography [34], and 70 eV was chosen for tungsten. However, in the previous works [32] the threshold displacement energy used was 128 eV, which was almost double the one used in nuclear data library JEFF3.3DPAarc. Therefore, this is the reason why the NRT_dpa values shown in this work are almost double the results presented in the previous works.

Considering tungsten as the test material in IFMIF-DONES, available integrated irradiation volume versus displacement damage dose rate have been calculated for different beam energies. In figure 8(*a*) the NRT_dpa calculations and the corresponding values, presented in table 4, for different positions and configuration of DEMO are shown as vertical lines. In this case, the specimen region volume in the HFTM has been considered. We can see that, depending on the energy of the IFMIF-DONES accelerator, one year or more of DEMO operation can be reproduced in one fpy of DONES. In the case of reproducing the data in the DIV, using a 25 MeV beam energy can be reproduced one fpy in this area in DEMO, and using a 40 MeV energy beam, almost 6 years of operation can be reproduced. However, the data in the FW are higher, and the 25 MeV beam energy cannot reproduce 1 fpy in this part of DEMO, being necessary at least 30 MeV beam energy. In figure 8(*b*), the primary displacement damage rate using the arc_dpa method is shown. As it can be seen, the behaviour in both panels is the same, but the range of values is lower for the arc_dpa method than for the NRT_dpa one as explained before.

The gas production to displacement damage ratio is a relevant quantity that presents the diffusion of displacement effects [20]. The unit used for the ratios are [H appm/dpa] and He/dpa [He appm/dpa].

In the case of He and H gas production for tungsten, the values obtained for each DEMO concept is very low, around 0.61–0.85 [He appm/NRT_dpa] and 1.42–2.0 [H appm/NRT_dpa] (tables 3 and 4). In the calculation of irradiation volumes as function of He-DPA and H-DPA for EUROFER97, usually only the four central rigs are taken into account since in the external ones the ratio is lower. In figure 9 the values obtained for DEMO are out of the range of IFMIF-DONES, being the production of He and H higher for DONES. So, in this case it seems interesting to obtain the ratios considering the whole HFTM volume. In figure 10 the gas production ratios are presented considering all the rigs.

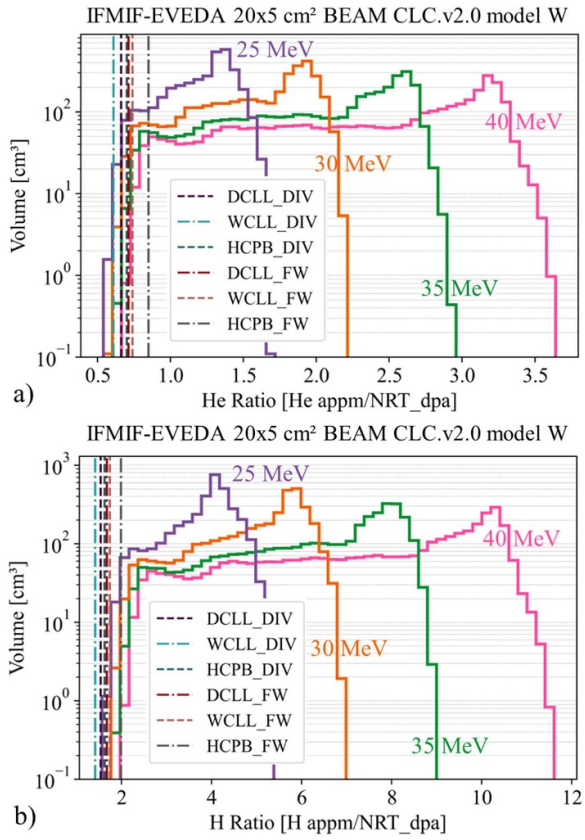

Figure 10. Irradiation volumes as function of He-DPA (panel (*a*)) and H-DPA (panel (*b*)) ratio for the CLC.v2.0 model for 20, 30, 35, 45 MeV energy beam and the values expected for each DEMO concept considering all the rigs.

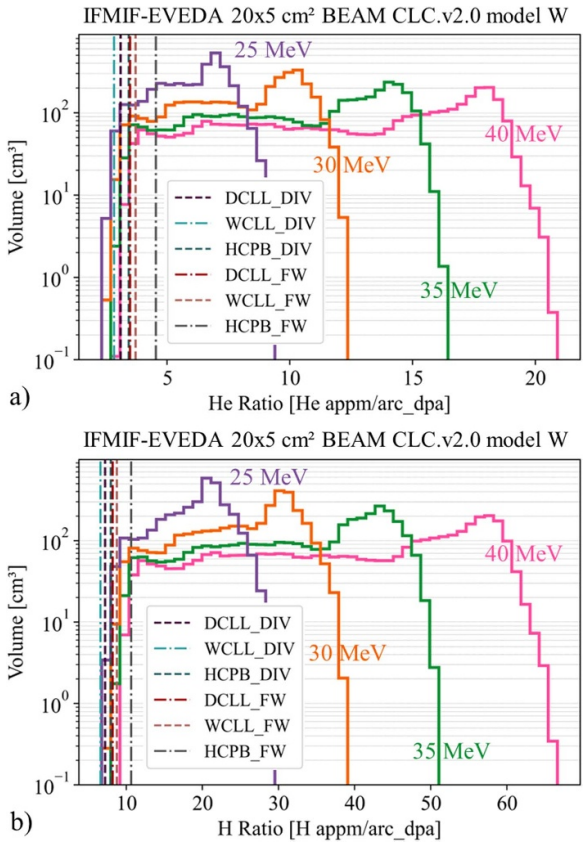

Figure 11. Irradiation volumes as function of He-DPA (panel (*a*)) and H-DPA (panel (*b*)) ratio for the CLC.v2.0 model for 20, 30, 35, 45 MeV energy beam and the values expected for each DEMO concept considering all the rigs.

For all the energies, the amount of volume with a lower ratio increases, maintaining the maximum peak volume. Now, the data of DEMO are just in the lower limit of these results. This indicates that at the level of gas production, tungsten does not meet the DEMO ratios in the central part of the HFTM. So, it appears interesting to consider placing the tungsten specimen in the farthest rigs from the beam.

The results of He and H production to primary displacement damage ratio using the arc_dpa method is shown in figure 11. The behaviour of the curves is completely similar to the previous one (figure 10), using the NRT_dpa model. The values of DEMO are just in the lower limit of the ratios calculated for all the rigs in the HFTM.

Taking as criteria the reproduction of the DEMO conditions in IFMIF-DONES concerning tungsten, the displacement damage rate values are fully satisfied and can be reproduced more than one year. Related to the gas production, there are parts of the HFTM that can satisfied the requirement of DEMO, but with a very low amount of volume.

3.2.2. CuCrZr alloy. Now, we have developed a similar study but considering that the specimens placed in the HFTM of IFMIF-DONES are made of CuCrZr alloy. First of all, in figure 12 the distribution of neutron fluence rate in a horizontal

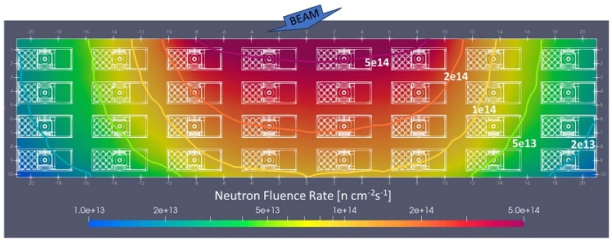

Figure 12. Horizontal cross section of the neutron fluence rate maps [ncm^{-2} s^{-1}] of CLC.v2.0 at the middle of the deuteron beam with CuCrZr alloy as specimen material.

map in the middle of the deuteron beam in the HFTM for a 20 × 5 cm^2 beam footprint size. As commented before, the neutron fluence rate is similar to the obtained with tungsten and for EUROFER [23, 32] because the volume considered is small and the influence of the change of material is not very noticeable.

In figure 13 is shown the statistic relative error for the 20 × 5 cm^2 beam footprint using CuCrZr alloy as material for the specimens in the CLC.v2.0 model. The range of the uncertainties are between 0.2% and 1%, is therefore considered a quality result based on [25].

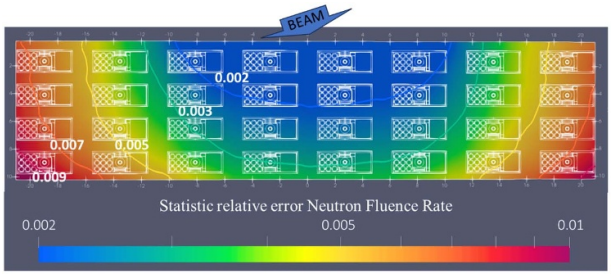

Figure 13. Horizontal cross section of the statistic relative error of the neutron fluence rate maps of the CLC.v2.0 model at the middle of the 20 × 5 cm^2 deuteron beam footprint size using CuCrZr alloy as specimens material.

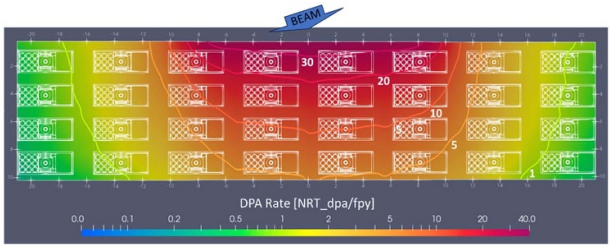

Figure 14. Horizontal cross section of the primary displacement damage rate [NRT_dpa/fpy] of the CLC.v2.0 specimen stacks at the middle of the deuteron beam with CuCrZr alloy as specimen material.

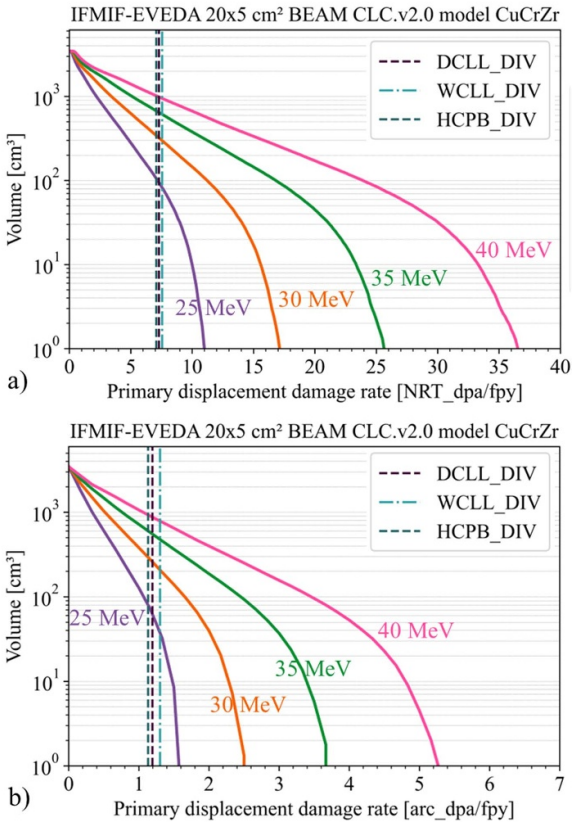

Figure 15. Available integrated irradiation volume (32 rigs) versus primary damage dose rate [dpa/fpy] for the CLC.v2.0 model for 20, 30, 35, 45 MeV energy beam and the values expected for each DEMO concept. (*a*) [NRT_dpa/fpy]; (*b*) [arc_dpa/fpy].

The primary displacement damage is determined by integrating the neutron flux with the CuCrZr dpa production cross-section. In figure 14 it can be seen the distribution of neutron fluence rate in a horizontal map in the middle of primary displacement damage rate for a 20 × 5 cm^2 beam footprint size. As the neutron fluence rate is higher in the central rigs (figure 12), the NRT_dpa values reached in this part are the highest. The range obtained is 0.2–37 [NRT_dpa/fpy]. This range is very similar to the obtained before in [32], with a maximum around 38 [NRT_dpa/fpy].

In figure 15 we show the primary displacement damage rate in NRT_dpa/fpy (panel (*a*)) and arc_dpa/fpy (panel (*b*)). Again, the tendency in both panels is the same, although the values reached are different, due to the calculation method. The DEMO values are around 7 [NRT_dpa/fpy] (table 5) and if using the 40 MeV beam energy in IFMIF-DONES, the highest value reached is around 37 [NRT_dpa/fpy], so, in this case, at least 5 fpy of DEMO can be reproduced in 1 fpy of IFMIF-DONES. Using the arc_dpa method, the DEMO values are around 1.2 [arc_dpa/fpy] (table 5) and if focusing in the 40 MeV beam energy in IFMIF-DONES, the highest value reached is around 6 [arc_dpa/fpy], so 5 fpy of DEMO can be reproduced in 1 fpy of IFMIF-DONES. So, the results with both calculation models are practically the same.

In figure 16 results of these ratios for He (panel (*a*)) and H (panel (*b*)) are shown. For these calculations only the volume of central part of the HFTM have been considered. We show the results for the four beam energies considered for IFMIF-DONES beam and the data expected in the DIV of the different DEMO configurations. The He ratios for DEMO are around 6.3–7 [He appm/NRT_dpa] (table 5) and these values are totally fulfilled for all the IFMIF-DONES beam energies except the lowest, 25 MeV. In the case of H ratio, the values for DEMO are around 35 [H appm/NRT_dpa] (table 5) and all the IFMIF-DONES beam energies fulfil this requirement.

Considering the arc_dpa method for calculating the gas production, the histogram presented in figure 17 is obtained. The He ratio for DEMO calculations are 26–45 [He appm/arc_dpa] (table 5) and this value is reached in all the energy range of the IFMIF-DONES beam, changing the amount of volume available. In the case of the H ratio, the DEMO values are 200–250 [H appm/arc_dpa] (table 5) and in this case also all IFMIF-DONES beam energies reach this value, but the nominal energy of 40 MeV is the one that produces the smallest volume at these values.

After showing the results for the CuCrZr alloy, all IFMIF-DONES beam energies fit well in terms of primary displacement damage rate, but for gas production the best performing energies are the lowest.

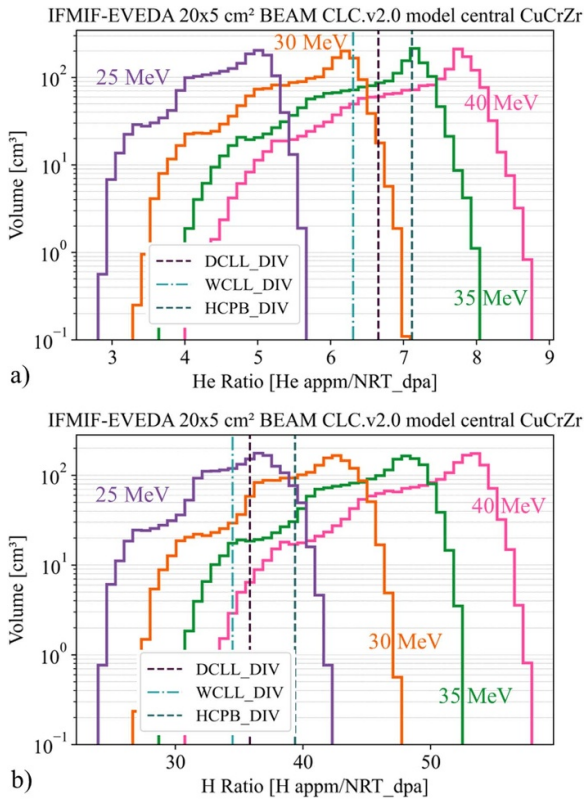

Figure 16. Central irradiation volumes as function of He-DPA ratio for the CLC.v2.0 model for 25, 30, 35, 45 MeV energy beam and the values expected for each DEMO.

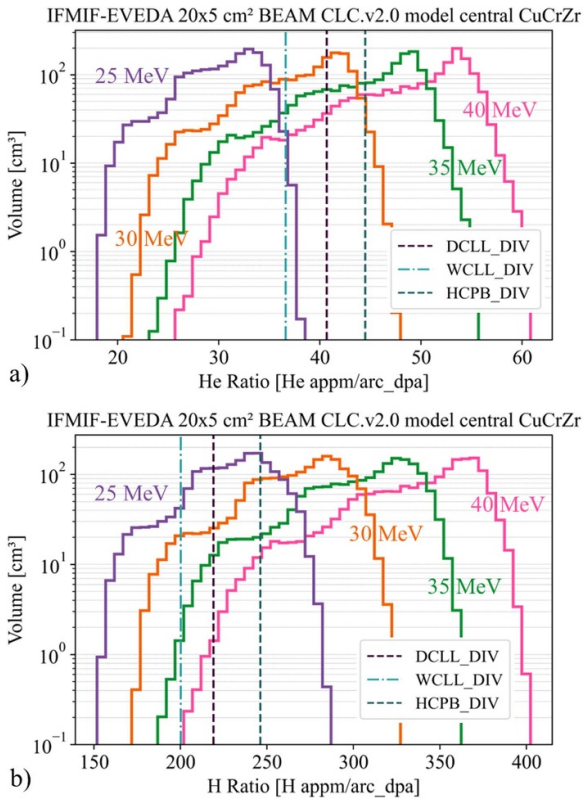

Figure 17. Central irradiation volumes as function of He-DPA (panel (*a*)) and H-DPA (panel (*b*)) ratio for the CLC.v2.0 model for 20, 30, 35, 45 MeV energy beam and the values expected for each DEMO concept considering the four central rigs.

4. Conclusions

In this paper calculations for different materials considered in the fusion roadmap for DEMO configuration are presented. These same data have been obtained for IFMIF-DONES, a facility that is going to reproduce the fusion reactor environment. Primary displacement damage ratio, and gas production have been compared for two cases. In the case of DEMO, different configurations such as DCLL, WCLL and HCPB, while for IFMIF-DONES, different beam energies have been considered. The materials of interest in this case have been tungsten and CrCuZr alloy.

For both materials, the primary displacement damage rate reached in IFMIF-DONES suits very well with the values expected in DEMO. In fact, the values reached in IFMIF-DONES are much higher. However, if the focus is on gas production, for CuCrZr alloy the data fit well both He and H rates; however, the gas production for tungsten in IFMIF-DONES is higher than in DEMO.

These results impact directly in how specimens can be placed in the HFTM depending on the material which they are made, in order to reproduce as best as possible, the environment in DEMO.

Acknowledgment

This work has been supported by the European Union's FEDER program, IFMIF-DONES Junta de Andalucia's program at the Universidad de Granada, by MCIN/AEI/10.13039/501100011033/FEDER, UE (PID2022-137543NB-I00) and has been carried out within the framework of the EUROfusion Consortium, funded by the European Union via the Euratom Research and Training Programme (Grant Agreement No. 101052200—EUROfusion). Views and opinions expressed are however those of the author(s) only and do not necessarily reflect those of the European Union or the European Commission. Neither the European Union nor the European Commission can be held responsible for them.

ORCID iDs

Irene Álvarez https://orcid.org/0000-0002-1654-3187
Fernando Mota https://orcid.org/0000-0002-1337-2482
David Sosa https://orcid.org/0009-0000-5319-5575
Iole Palermo https://orcid.org/0000-0001-8725-8167

References

[1] Knaster J., Moeslang A. and Muroga T. 2016 Materials research for fusion *Nat. Phys.* **12** 424–34

[2] Deng C., Liu M., Yang Z., Deng C., Zhou K., Kuang Z and Zhang J 2014 Manufacture of thick VPS W coatings on relatively large CuZrCr substrate and its steady high heat load performance *J. Nucl. Mater.* **455** 145–50

[3] Romanelli F. 2012 A roadmap to the realisation of fusion energy www.efda.org (EFDA Leader) (available at: www.eurofusion.org/wpcms/wp-content/uploads/2013/01/JG12.356-web.pdf)

[4] Fabritsiev S.A., Zinkle S.J. and Singh B.N. 1996 Evaluation of copper alloys for fusion reactor divertor and first wall components *J. Nucl. Mater.* **233–7** 127–37

[5] Barabash V.R., Kalinin G.M., Fabritsiev S.A. and Zinkle S.J. 2011 Specification of CuCrZr alloy properties after various thermo-mechanical treatments and design allowables including neutron irradiation effects *J. Nucl. Mater.* **417** 904–7

[6] Hernández-Pérez A., Eddahbi M., Monge M.A., Muñoz A. and Savoini B. 2015 Microstructure and mechanical properties of an ITER-grade Cu–Cr–Zr alloy processed by equal channel angular pressing *Fusion Eng. Des.* **98–9** 1978–81

[7] Stork D. *et al* 2014 Materials R&D for a timely DEMO: key findings and recommendations of the EU Roadmap Materials Assessment Group *Fusion Eng. Des.* **89** 1586–94

[8] Fabritsiev S.A. *et al* 2009 Effect of irradiation temperature and dose on mechanical properties and fracture characteristics of Cu//SS joints for ITER *J. Nucl. Mater.* **386–8** 824–9

[9] Knaster J. *et al* 2016 The accomplishment of the engineering design activities of IFMIF/EVEDA: the European–Japanese project towards a Li(d,xn) fusion relevant neutron source *Nucl. Fusion* **55** 086003

[10] Ibarra A., Heidinge R., Barabaschi P., Mota F., Mosnier A., Cara P. and Nitti F.S. 2014 A stepped approach from IFMIF/EVEDA toward IFMIF *Fusion Sci. Technol.* **66** 252–9

[11] Bernardi D. *et al* 2019 Towards the EU fusion-oriented neutron source: the preliminary engineering design of IFMIF-DONES *Fusion Eng. Des.* **146** 261–8

[12] Qiu Y. *et al* 2024 Overview of recent advancements in IFMIF-DONES neutronics activities *Fusion Eng. Des.* **201** 114242

[13] Fernández-Berceruelo I. *et al* 2021 Alternatives for upgrading the EU DCLL breeding blanket from MMS to SMS *Fusion Eng. Des.* **167** 112380

[14] Rapisarda D. *et al* 2021 The European Dual Coolant Lithium Lead breeding blanket for DEMO: status and perspectives *Nucl. Fusion* **61** 115001

[15] Arena P. *et al* 2021 The DEMO water-cooled lead–lithium breeding blanket: design status at the end of the pre-conceptual design phase *Appl. Sci.* **11** 11592

[16] Moro F. *et al* 2021 Nuclear performances of the water-cooled lithium lead DEMO reactor: neutronic analysis on a fully heterogeneous model *Fusion Eng. Des.* **168** 112514

[17] Palermo I., Hernández F.A., Pereslavtsev P., Rapisarda D. and Zhou G. 2022 Shielding design optimization of the helium-cooled pebble bed breeding blanket for the EU DEMO fusion reactor *Energies* **15** 5734

[18] Zhou G. *et al* 2023 The European DEMO Helium Cooled Pebble Bed breeding blanket: design status at the conclusion of the pre-concept design phase *Energies* **16** 5377

[19] Zhou G. *et al* 2023 Design update of the European DEMO Helium Cooled Pebble Bed breeding blanket *CBBI-21* (*Granada, Spanien*, *19–20 Oktober*) (available at: https://publikationen.bibliothek.kit.edu/1000165661)

[20] Odette G.R., Maziasz P.J. and Spitznagel J.A. 1981 Fission-fusion correlations for swelling and microstructure in stainless steels: effect of the helium to displacement per atom ratio *J. Nucl. Mater.* **104** 1289–304

[21] Qiu Y., Arbeiter F., Fischer U. and Schwab F. 2018 IFMIF-DONES HFTM neutronics modeling and nuclear response analyses *Nucl. Mater. Energy* **15** 185–9

[22] Álvarez I., Anguiano M., Mota F., Hernández R. and Qiu Y. 2024 Neutronic assessment of the IFMIF-DONES HFTM specimen stack distribution *Fusion Eng. Des.* **200** 114212

[23] Álvarez I. *et al* 2025 Comparative analysis of neutronic features for various specimen payload configurations within the IFMIF-DONES *HFTM Fusion Eng. Des.* **210** 114729

[24] Arbeiter F., Abou-Sena A., Chen Y., Dolensky B., Heupel T., Klein C., Scheel N. and Schlindwein G. 2011 Development and validation status of the IFMIF high flux test module *Fusion Eng. Des.* **86** 2011

[25] Serrano M., Hernández R., Plaza D., Muñoz A., Castellanos J. and Molla J. 2011 *Assessment of SSTT Technology* (available at: https://idm.euro-fusion.org/default.aspx?uid=2MLMCM)

[26] Werner C.J. *et al* 2018 MCNP version 6.2 release notes (LA-UR-18-20808) (Los Alamos National Laboratory) (available at: https://laws.lanl.gov/vhosts/mcnp.lanl.gov/pdf_files/la-ur-18-20808.pdf)

[27] Konobeyev A., Korovin Y.A., Pereslavtsev P.E., Fischer U. and von Möllendorff U. 2001 Development of methods for calculation of deuteron-lithium and neutron-lithium cross sections for energies up to 50 MeV *Nucl. Sci. Eng.* **139** 1–23

[28] IAEA - International Atomic Energy Agency FENDL-3.1d: fusion evaluated nuclear data library *Ver.3.1d* (available at: www-nds.iaea.org/fendl/)

[29] Norgett M.J., Robinson M.T. and Torrens I.M. 1975 A proposed method of calculating displacement dose rates *Nucl. Eng. Des.* **33** 50–54

[30] Nordlund K. *et al* 2018 Improving atomic displacement and replacement calculations with physically realistic damage models *Nat. Commun.* **9** 1084

[31] Nuclear Energy Agency JEFF3.3DPAarc (available at: www.oecd-nea.org/dbdata/jeff/jeff33/index.html#dpa)

[32] Fischer U. and Qiu Y. 2020 Material compositions for PPPT neutronics and activation analyses *EUROfusion IDM EFDA_2MM3A6 v1.2* (available at: https://idm.euro-fusion.org/default.aspx?uid=2MM3A6)

[33] Mota F., Palermo I., Laces S., Molla J. and Ibarra A. 2017 Potential irradiation of Cu alloys and tungsten samples in DONES *Nucl. Fusion* **57** 126056

[34] Konobeyev A.Y., Fischer U., Korovin Y.A. and Simakov S.P. 2017 Evaluation of effective threshold displacement energies and other data required for the calculation of advanced atomic displacement cross-sections *Nucl. Energy Technol.* **3** 169–75